Supplement

Changing phytoplankton phenology in the marginal ice zone west of the Antarctic Peninsula

Jessica S. Turner[1,*], Heidi Dierssen[1], Oscar Schofield[2], Heather H. Kim[3], Sharon Stammerjohn[4], David R. Munro[4,5], Maria Kavanaugh[6]

[1] Department of Marine Sciences, University of Connecticut, Groton, CT 06340, USA.
[2] Department of Marine and Coastal Sciences, Rutgers University, New Brunswick, NJ 08901, USA.
[3] Department of Marine Chemistry and Geochemistry, Woods Hole Oceanographic Institution, Woods Hole, MA 02453, USA.
[4] Cooperative Institute for Research in Environmental Sciences, University of Colorado, Boulder, CO 80309, USA.
[5] National Oceanic and Atmospheric Administration, Global Monitoring Laboratory, Boulder, CO 80309, USA.
[6] College of Earth, Ocean, and Atmospheric Sciences, Oregon State University, Corvallis, OR 97331, USA.
*Corresponding author, email: jturner@uconn.edu

Contents of this file:

Figs. S1–S18

Introduction

The supporting information in this file includes: January monthly coverage of Coastal Zone Color Scanner (CZCS) chlorophyll-a concentration (Chl-a) data (Fig. S1) and January 1981 daily coverage of CZCS Chl-a data (Fig. S2) as referenced by Montes-Hugo et al. 2009, NEW (Fig. S3) comparison of global algorithm Chl-a and corrected Southern Ocean Chl-a to match field data (Fig. S4), transect of in situ field data and satellite-derived Chl-a algorithms across the Drake Passage (Fig. S5), data availability of CMEMS GlobColour Chl-a data used in the paper in terms of overall coverage (Fig. S6) and data availability by month (Fig. S7), change-point analysis for time series of bloom start date (Fig. S8) and bloom peak date (Fig. S9), sensitivity tests for phytoplankton bloom start date calculations (Fig. S10), spatial percent of data per year removed from analysis due to no distinctive bloom (Fig. S11), overall Chl-a concentration by region (Fig. S12), decadal wind speed and direction (Fig. S13), decadal seasonal cycles of daily photosynthetically active radiation (PAR) (Fig. S14), trends in PAR by month 1997-2022 (Fig. S15), decadal seasonal cycles of daily sea surface temperature (SST) (Fig. S16), trends in SST by month 1997-2022 (Fig. S17), and sea ice retreat and advance trends (Fig. S18).

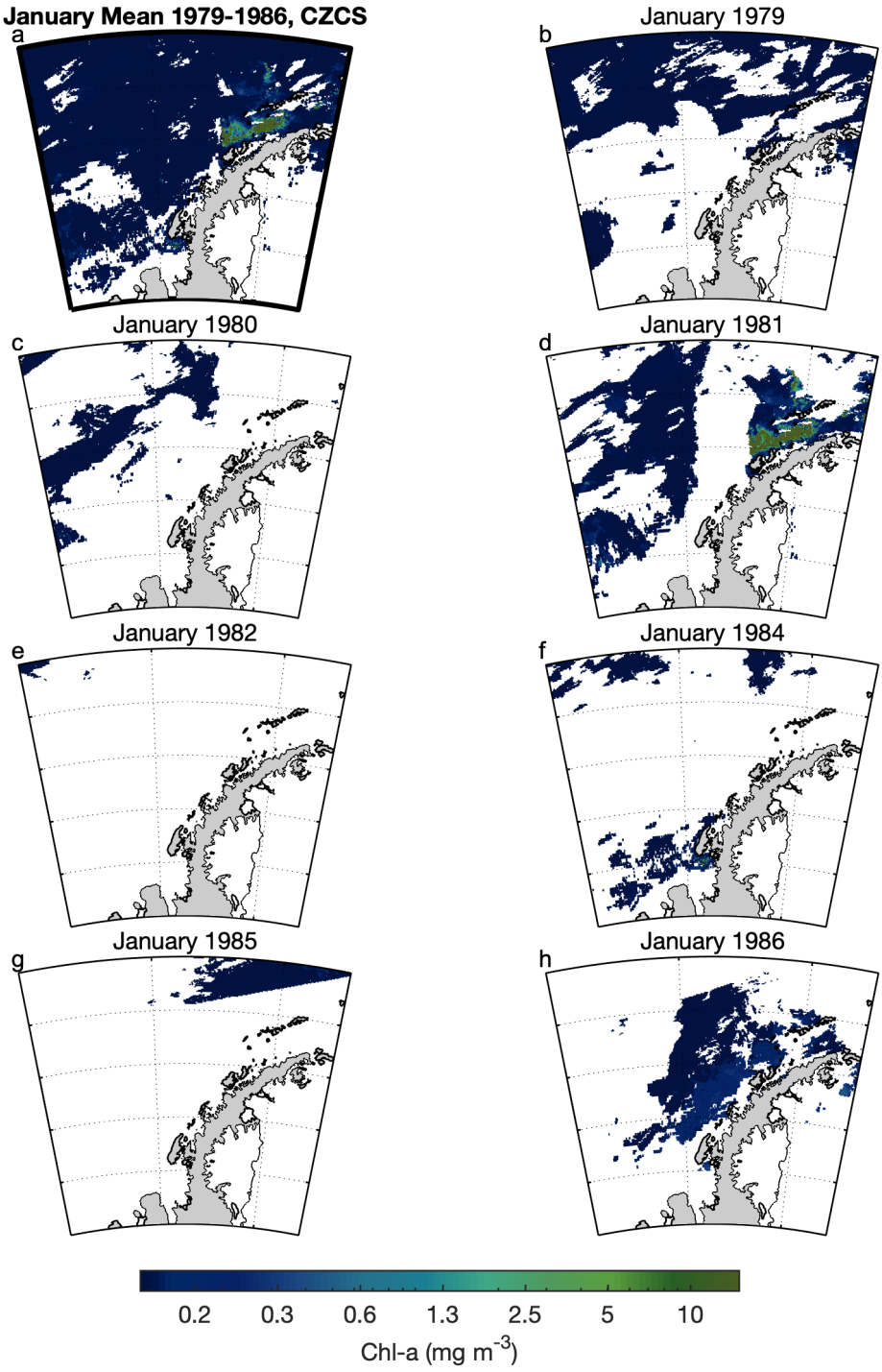

Fig. S1. January coverage of CZCS Chl-a data 1979 to 1986 as referenced by Montes-Hugo et al. (2009), including a) Mean Chl-a for January 1979 to 1986 (bolded), and b-h) January means for years 1979, 1980, 1981, 1982, 1984, 1985, and 1986. No data were available for January 1983.

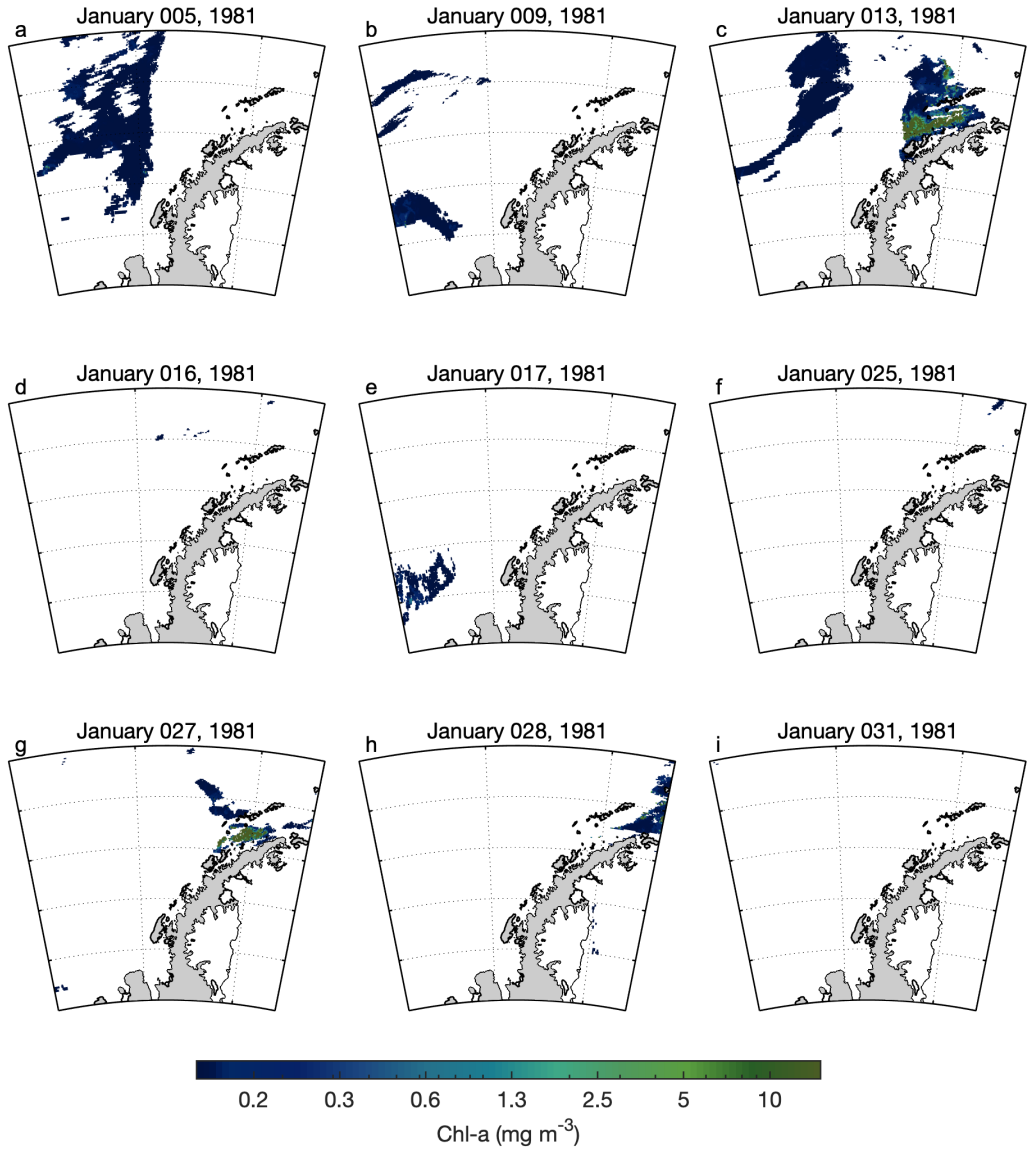

Fig. S2. Coverage of all available January 1981 CZCS Chl-a data as referenced by Montes-Hugo et al. (2009).

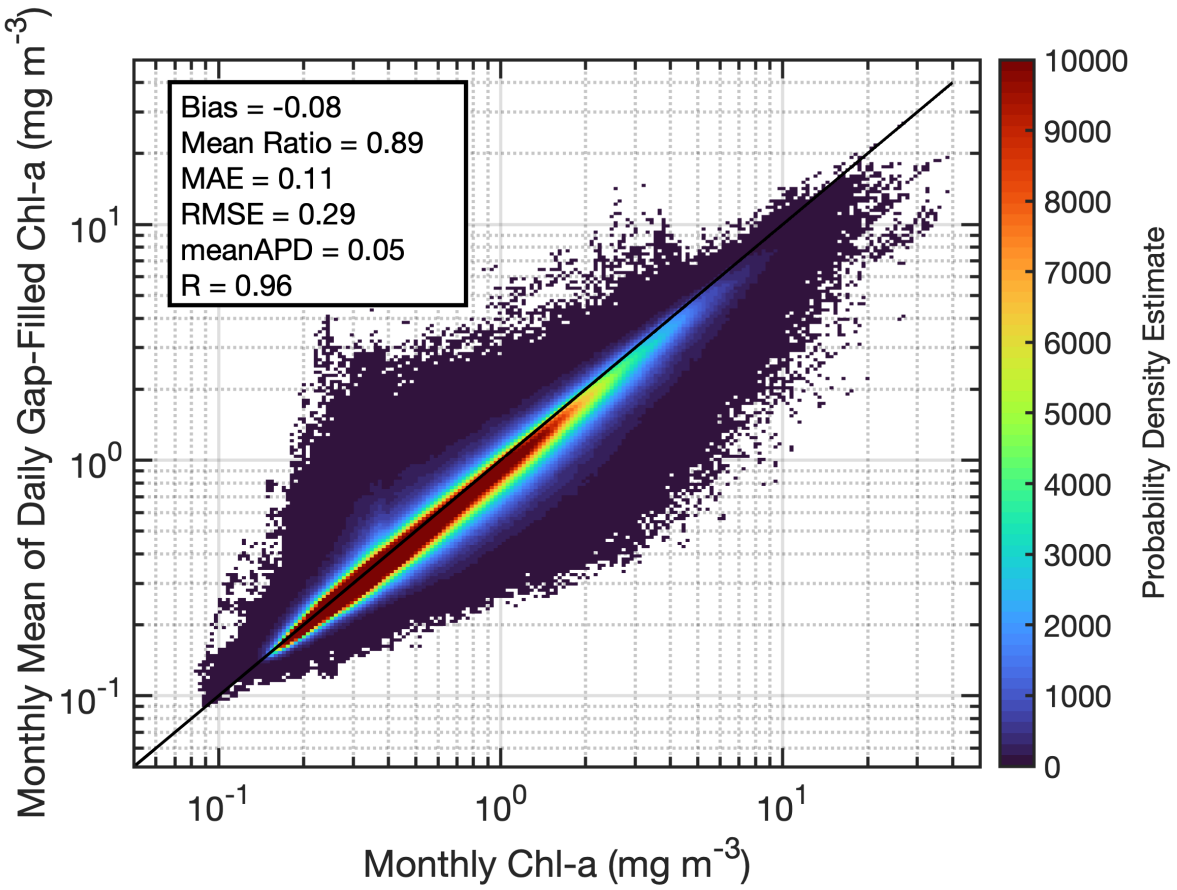

Fig. S3. Comparison of the monthly mean of gap-filled daily Chl-a concentration to the non-gap-filled monthly mean Chl-a concentration from CMEMS GlobColour for 1997-2022 in the west Antarctic Peninsula region (i.e., all pixels in the region -55 to -80°W and -60 to -70°S).

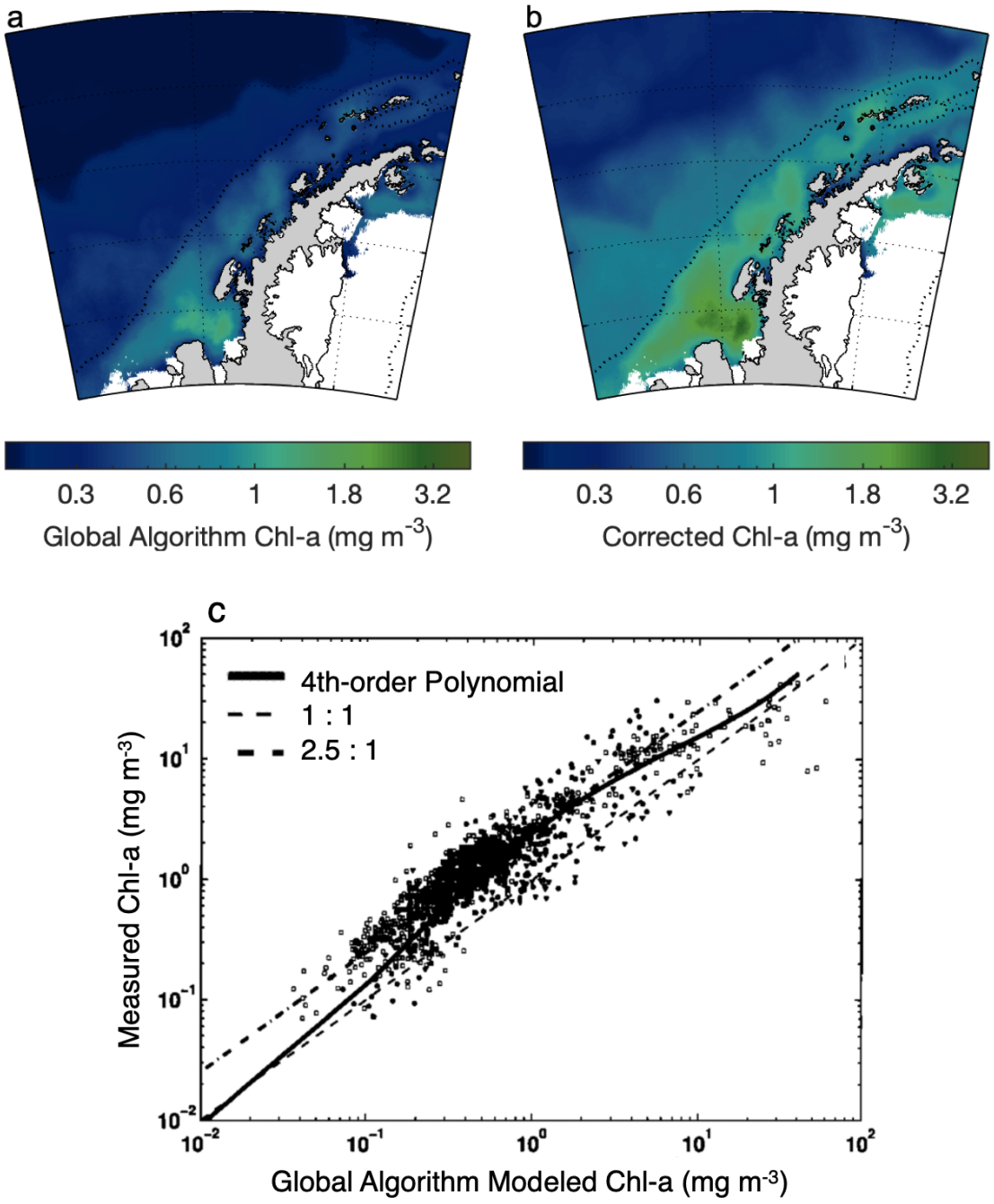

Fig. S4. a) Global algorithm Chl-a and b) corrected Chl-a using the 4th-order polynomial to match field data, as global algorithms underestimate in situ WAP Chl-a by a factor of 2 to 2.5 as seen in: c) Measured Chl-a vs. modeled Chl-a from the OC2V2 global algorithm, adapted from Dierssen and Smith (2000) Fig. 8B. The dashed line represents a 1:1 correlation and the dot-dashed line represents a 2.5:1 correlation. The thick black line represents corrected Chl-a using the 4th-order polynomial applied to the global algorithm:

$$Chl_{corrected} = 10^{(0.3914 + 1.0176X - 0.3114X^2 + 0.0186X^3 + 0.0610X^4)}$$

where $X = \log(Chl_{global})$.

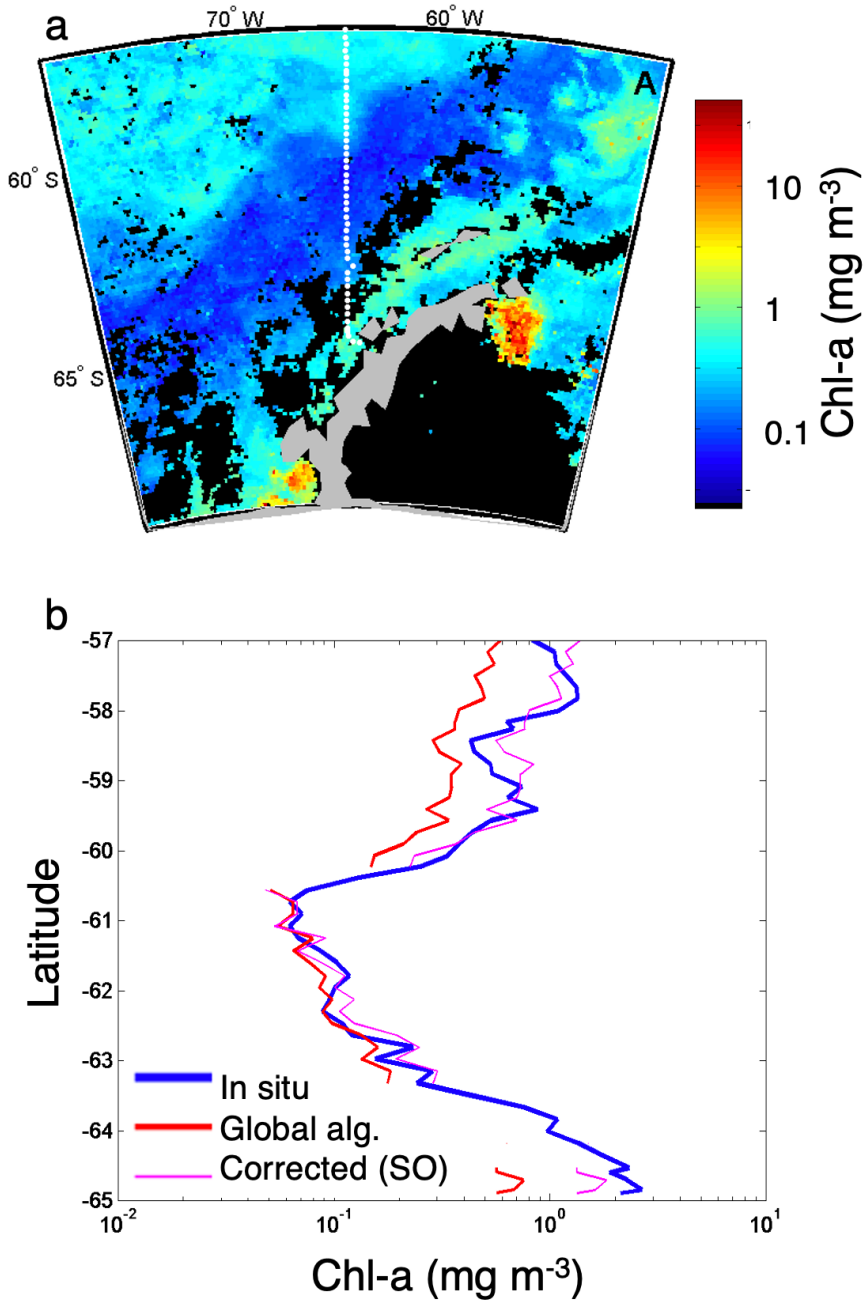

Fig. S5. a) SeaWiFS-derived Chl-a from January 1999 corrected with regional Southern Ocean (SO) algorithm across a portion of the Drake Passage between South America and the Antarctic Peninsula. b) In situ Chl-a from water samples collected underway from the *R/V Laurence M. Gould* using standard fluorometric techniques (Smith et al. 1981) (Blue) compared with SeaWiFS standard OC2V2 global algorithm Chl-a (Red) and SO-corrected SeaWiFS Chl-a (Pink). The SeaWiFS lines are non-contiguous in areas that were cloud covered during all satellite overpasses for that month. Adapted from Dierssen (2000).

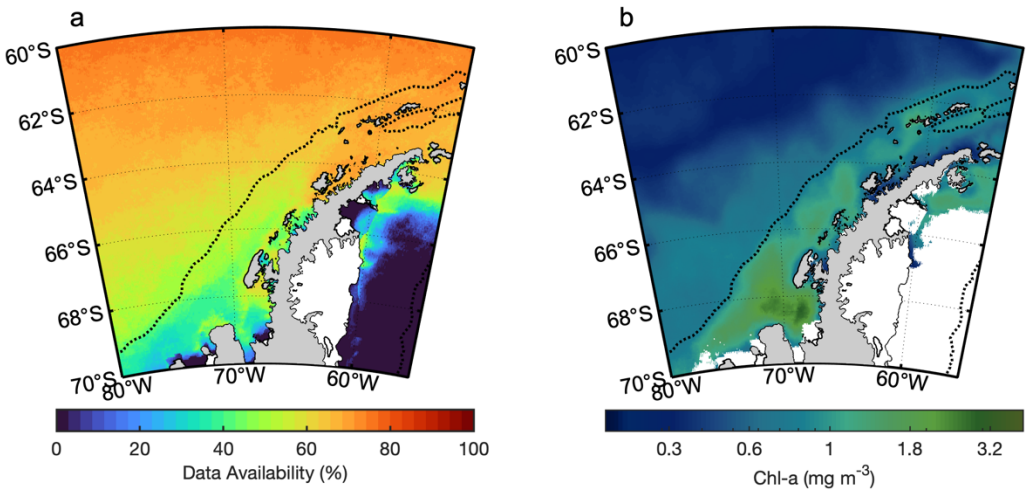

Fig. S6. a) Data availability in terms of percent temporal coverage from CMEMS GlobColour Level-4 daily Chl-a data. b) Long-term mean accumulation season Chl-a from daily Level-4 data for the available time series September 1997 to June 2022. White areas in b) show where spatial points with less than 30% temporal coverage were excluded from further analysis. Black dotted line indicates the continental shelf break (1000 m isobath).

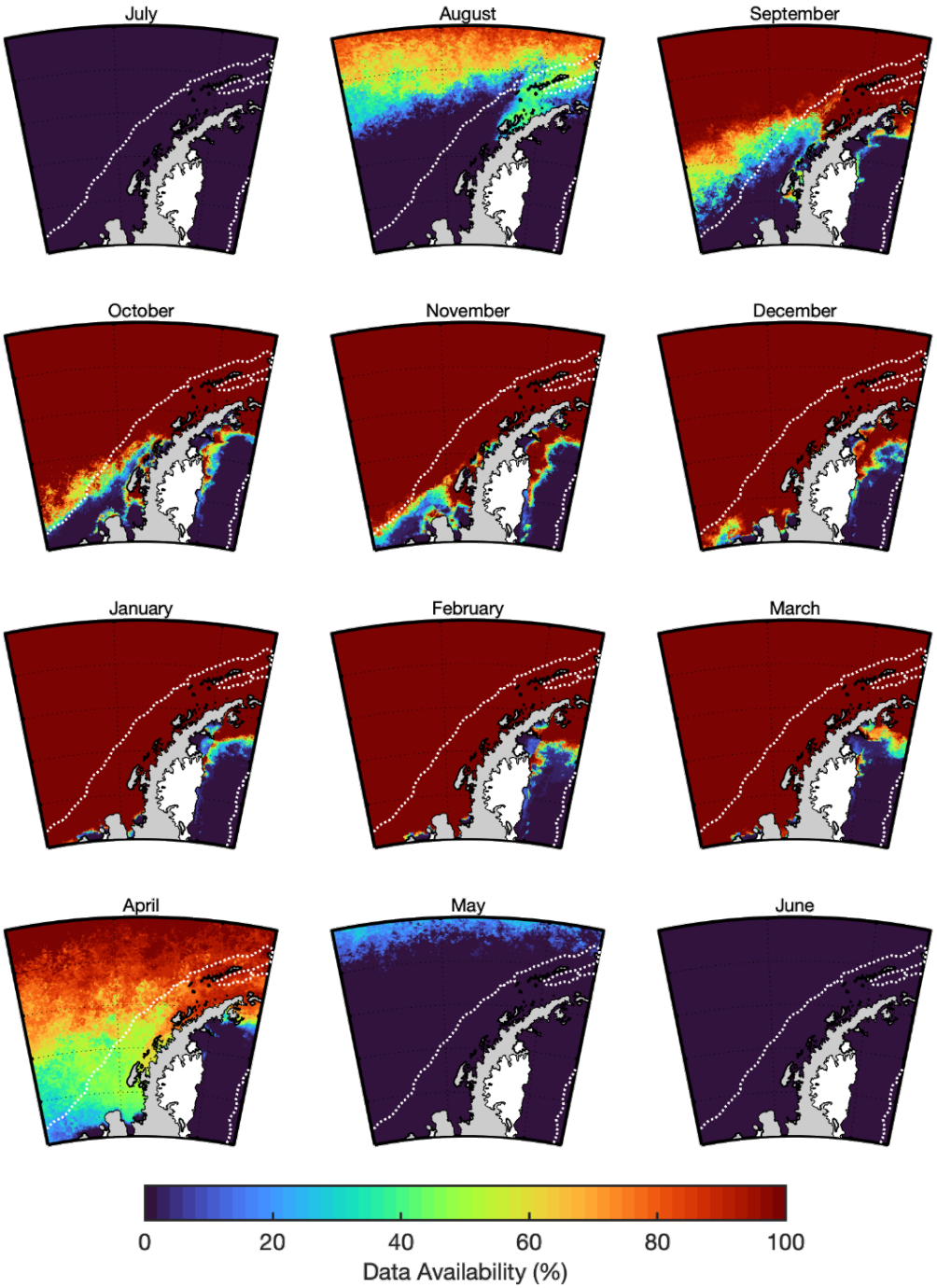

Fig. S7. Data availability in terms of percent temporal coverage from monthly means of daily Chl-a data. Spatially, color indicates relative number of daily scenes for which data are available for each month throughout the 24-year time series (e.g., 1 = 100% of 744 daily scenes for a 31-day long month). White dotted line indicates the continental shelf break (1000 m isobath).

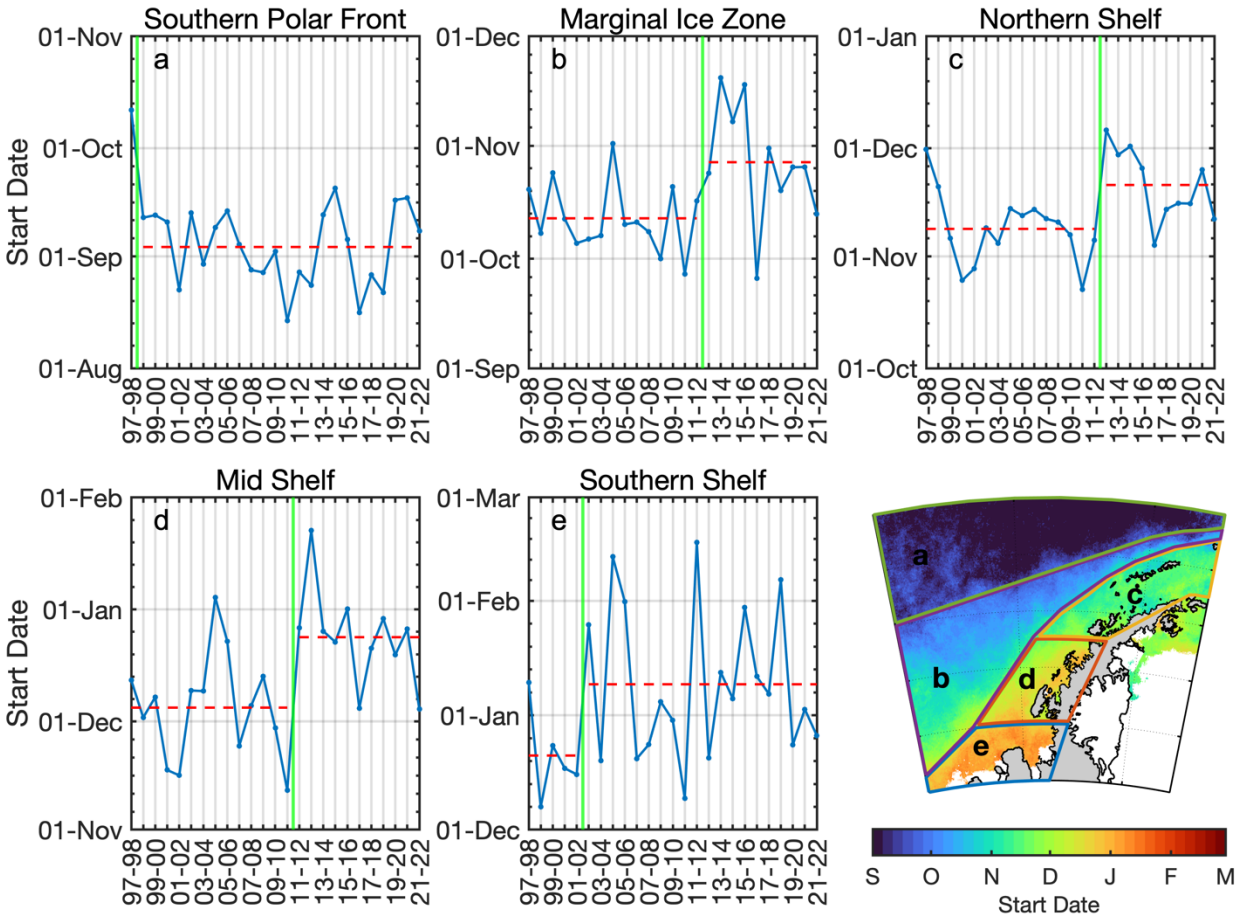

Fig. S8. Change-point analysis for start dates for each ecoregion 1997-2022. Blue lines show each start date time series, green lines indicate the change-point in each time series, and red dotted lines indicate the means before and after the change-point. Map inset shows ecoregion locations overlaying long-term mean start date, with letters indicating the first day of the month (e.g., "S" for 1 September).

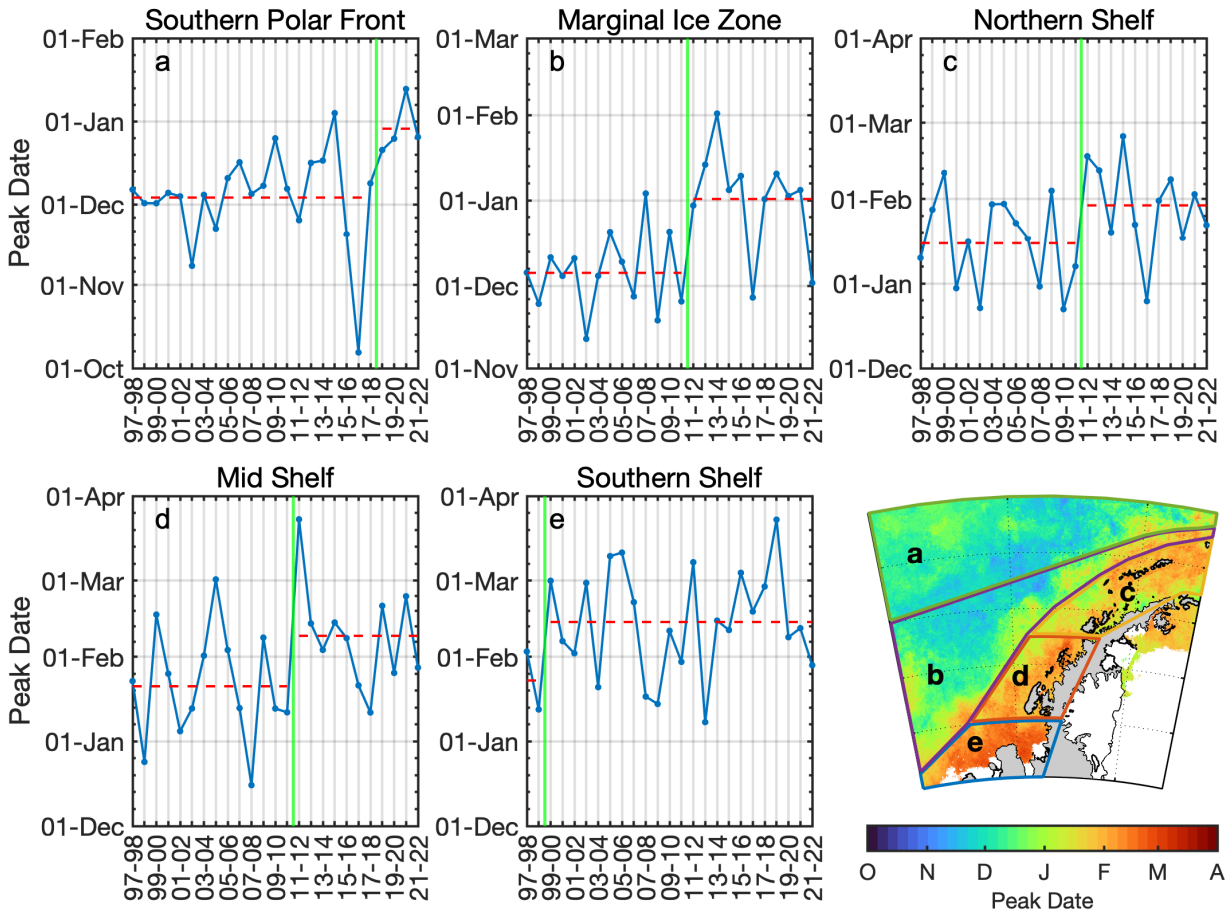

Fig. S9. Change-point analysis for peak dates for each ecoregion 1997-2022. Blue lines show each peak date time series, green lines indicate the change-point in each time series, and red dotted lines indicate the means before and after the change-point. Map inset shows ecoregion locations overlaying long-term mean peak date, with letters indicating the first day of the month (e.g., "N" for 1 November).

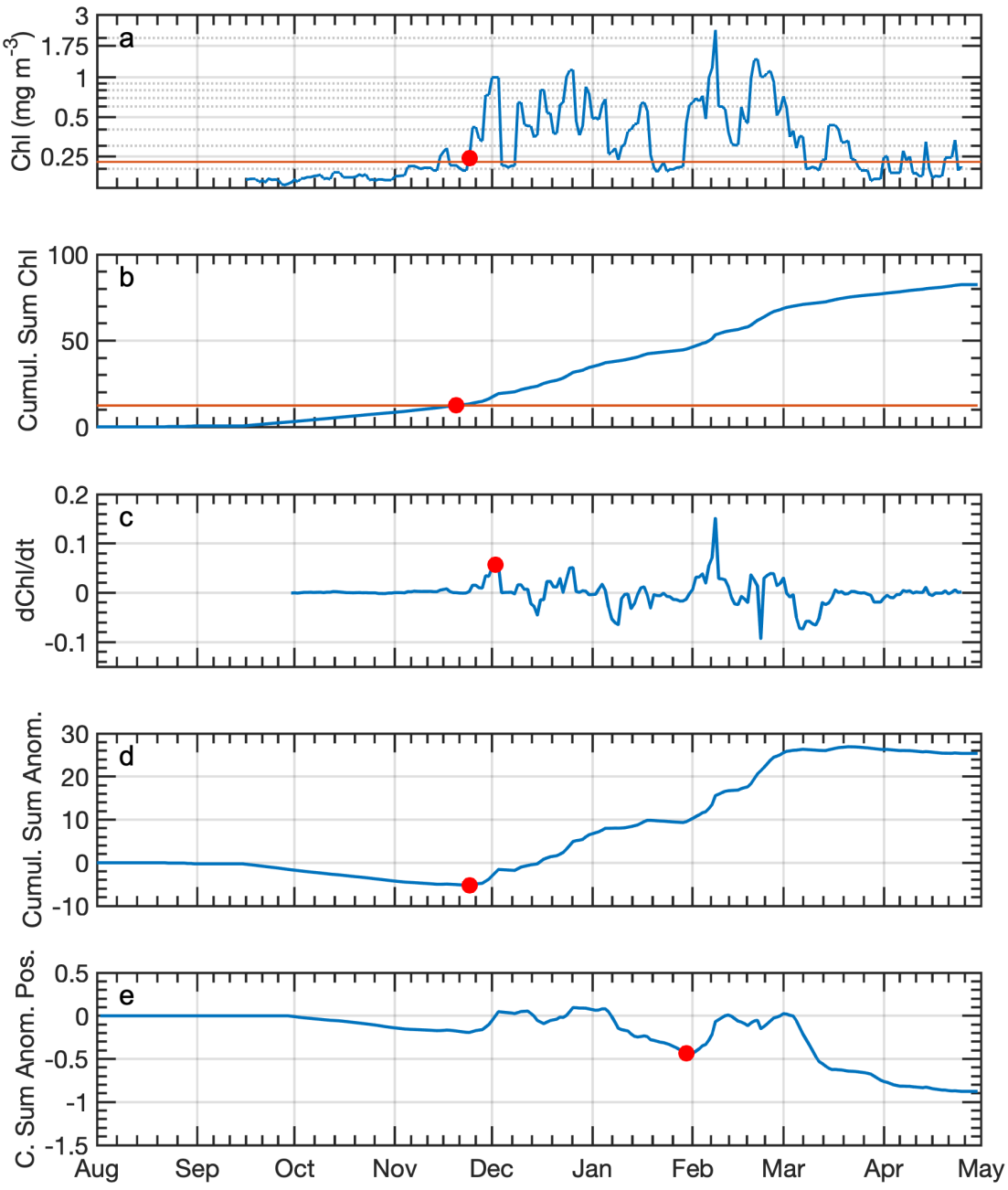

Fig. S10. Sensitivity test for bloom start date calculations, at example Palmer Station E, 2006-2007 for the indices: a) Threshold, b) Cumulative Sum, c) Rate of Change, d) Cumulative Sum of Anomalies, e) Cumulative Sum of Anomalies of Positive Growth, as in Thomalla et al. (2015). Bloom start dates are, respectively: 24 Nov, 29 Nov, 2 Dec, 24 Nov, and 30 Jan. From these sensitivity tests, the Threshold approach was chosen as the most representative index. Spatially, the Threshold method showed the clearest gradient from offshore to onshore and from north to south in the average timing of the start of the bloom across all years. The Threshold method fell in the middle of the distribution of all indices in terms of resulting trends over time.

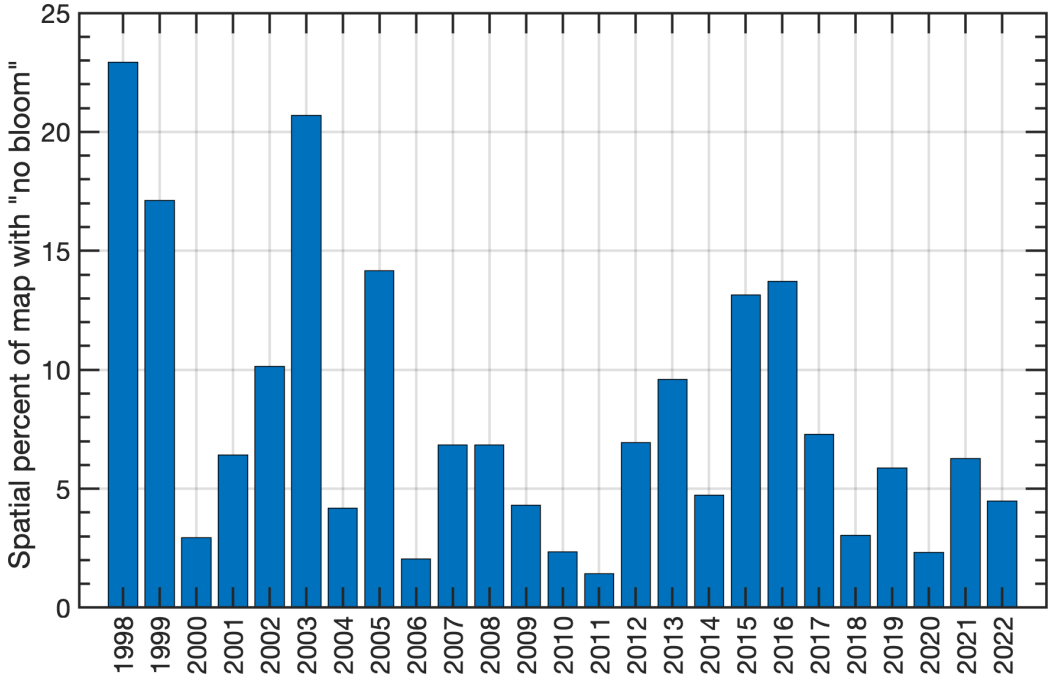

Fig. S11. Spatial percent of data for each year of the entire study region that was excluded from phenology analysis due to lack of a substantial bloom, in terms of percent of all grid locations. Locations that experienced "no bloom" for a given year had Chl-a never exceeding 2.5 times the long-term threshold value (where the threshold value is the long-term median plus 5%, i.e., 0.4 mg m^{-3} for the mid shelf). 19 of 25 years experienced a substantial bloom for > 90% of the ocean area analyzed.

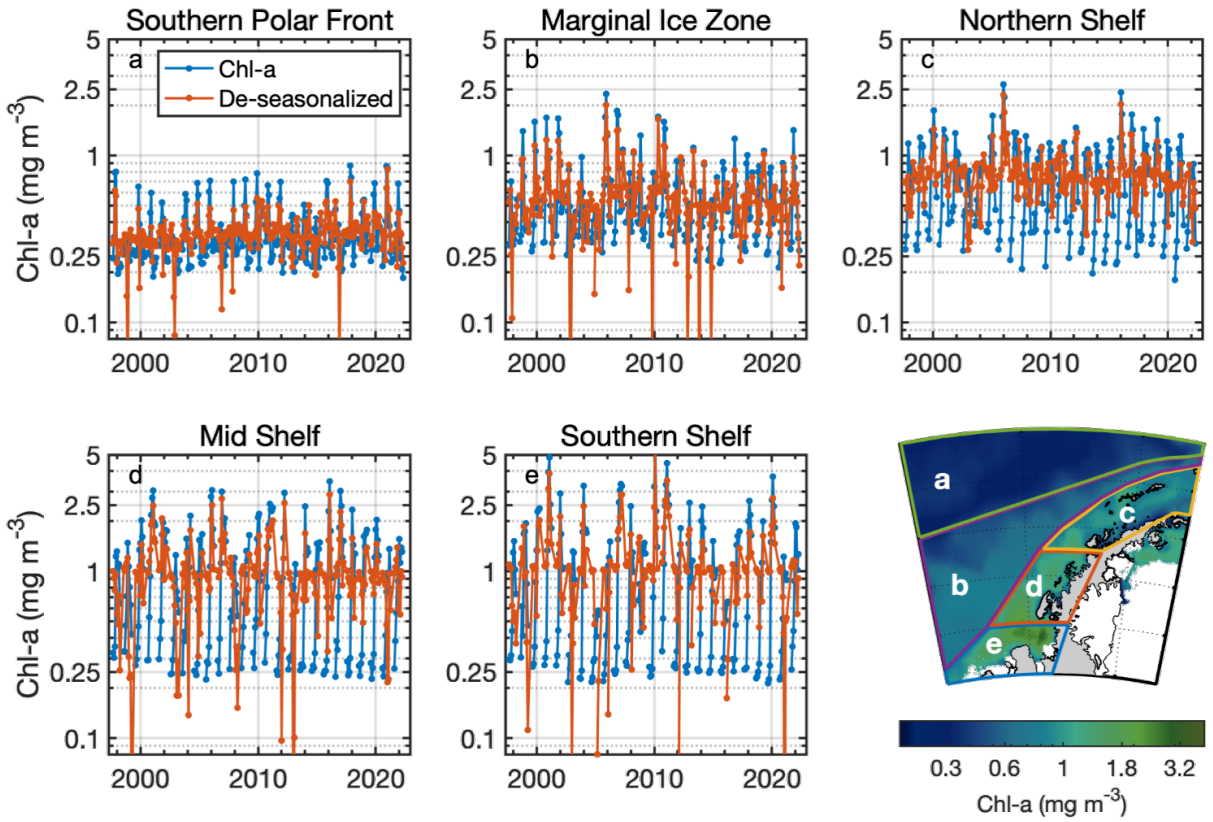

Fig. S12. Trends in regionally averaged, de-seasonalized monthly Chl-a in regions a) Southern Polar Front, b) Marginal Ice Zone, c) Northern Shelf, d) Mid Shelf, and e) Southern Shelf. Map inset shows long-term mean Chl-a concentration 1997-2022 with regions overlaid. De-seasonalizing was performed using the Climate Data Toolbox *deseason* function in MATLAB R2019a (Greene et al. 2019). The function detrends the original data to isolate the seasonal component, then subtracts the seasonal component from the original data:

$$y = y_0 + y_{tr} + y_{season} + y_{var} + y_{noise}$$

$$y_{de-seasonalized} = y - y_{season}$$

where y is the original data, y_0 is the long-term mean, y_{trend} is the long-term trend, y_{season} is the typical seasonal anomaly, which the function obtains after detrending and removing the mean, y_{var} represents interannual variability, and y_{noise} is the residual.

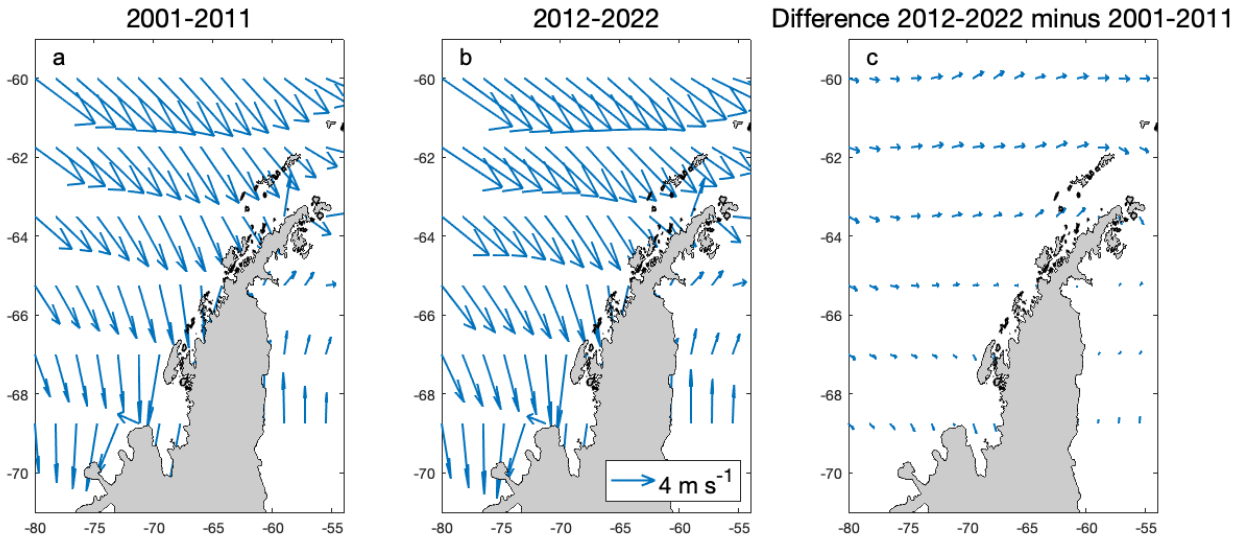

Fig. S13. Average wind speed and wind direction for a) 2001-2011, b) 2012-2022, and c) the difference in the u,v wind components from 2012-2022 minus those from 2001-2011.

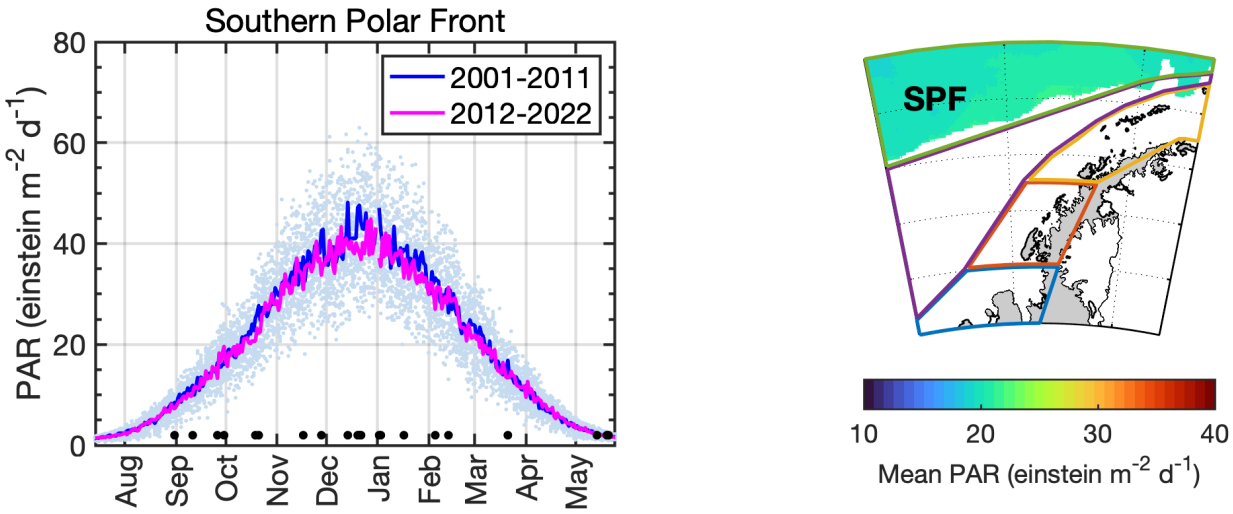

Fig. S14. Seasonal cycles of daily PAR for two decades 2000-2010 (blue) vs. 2010-2020 (pink) for the Southern Polar Front (SPF) ecoregion where sea ice cover does not impact PAR retrievals from satellite. Black dots along x axis indicate the 16 days for which decades were significantly different, dispersed throughout the season ($p < 0.049$; Kruskal-Wallis). For all other 349 days of the year, decades were not significantly different ($p > 0.059$; Kruskal-Wallis). Map inset shows the SPF ecoregion overlaying long-term mean PAR 1997-2022.

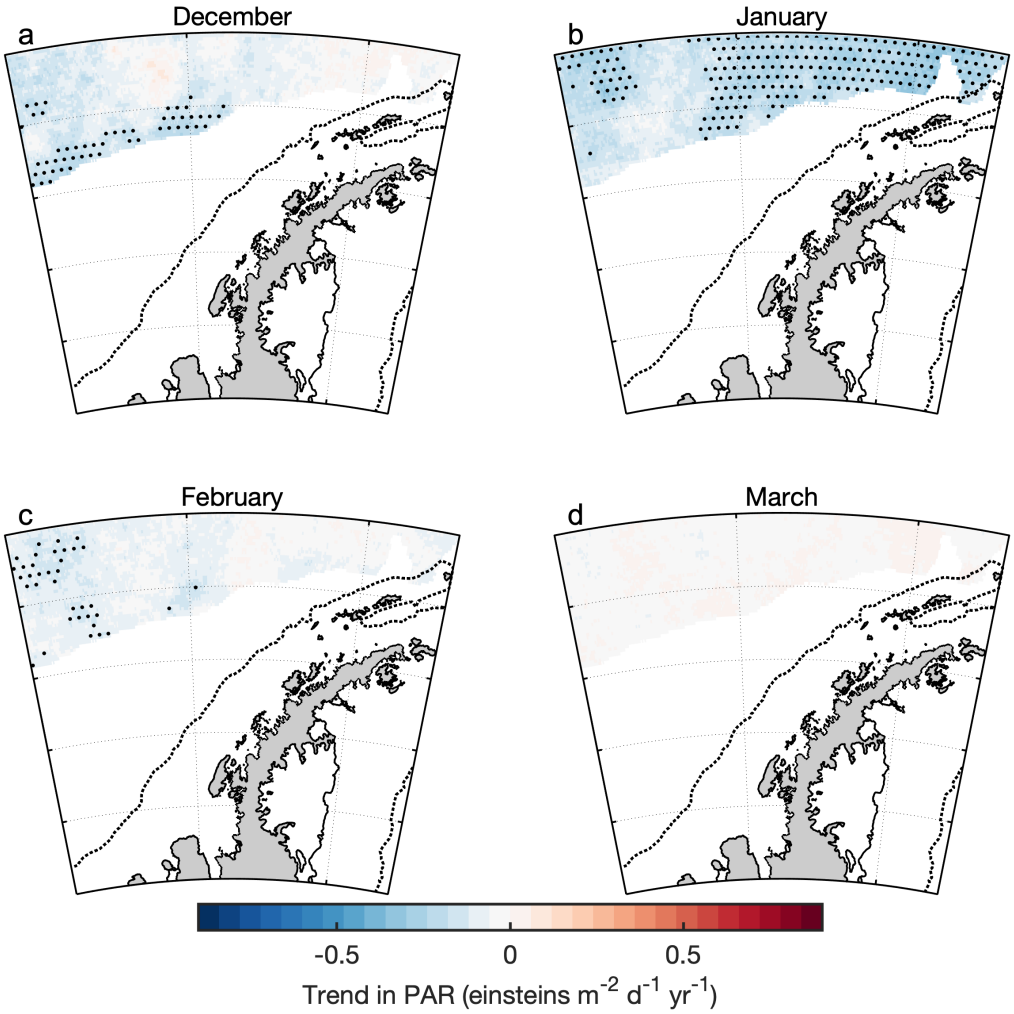

Fig. S15. Trends in PAR for each month over the 25-year time series. Analysis was limited to only the Southern Polar Front (SPF) ecoregion where sea ice cover does not impact PAR retrievals from satellite. Analysis was limited to December-March months when sea ice cover does not impact PAR retrievals from satellite. Stippling indicates areas where trends are statistically significant ($p < 0.05$; Theil-Sen nonparametric estimator of slope). Black dotted line indicates the continental shelf break (1000 m isobath).

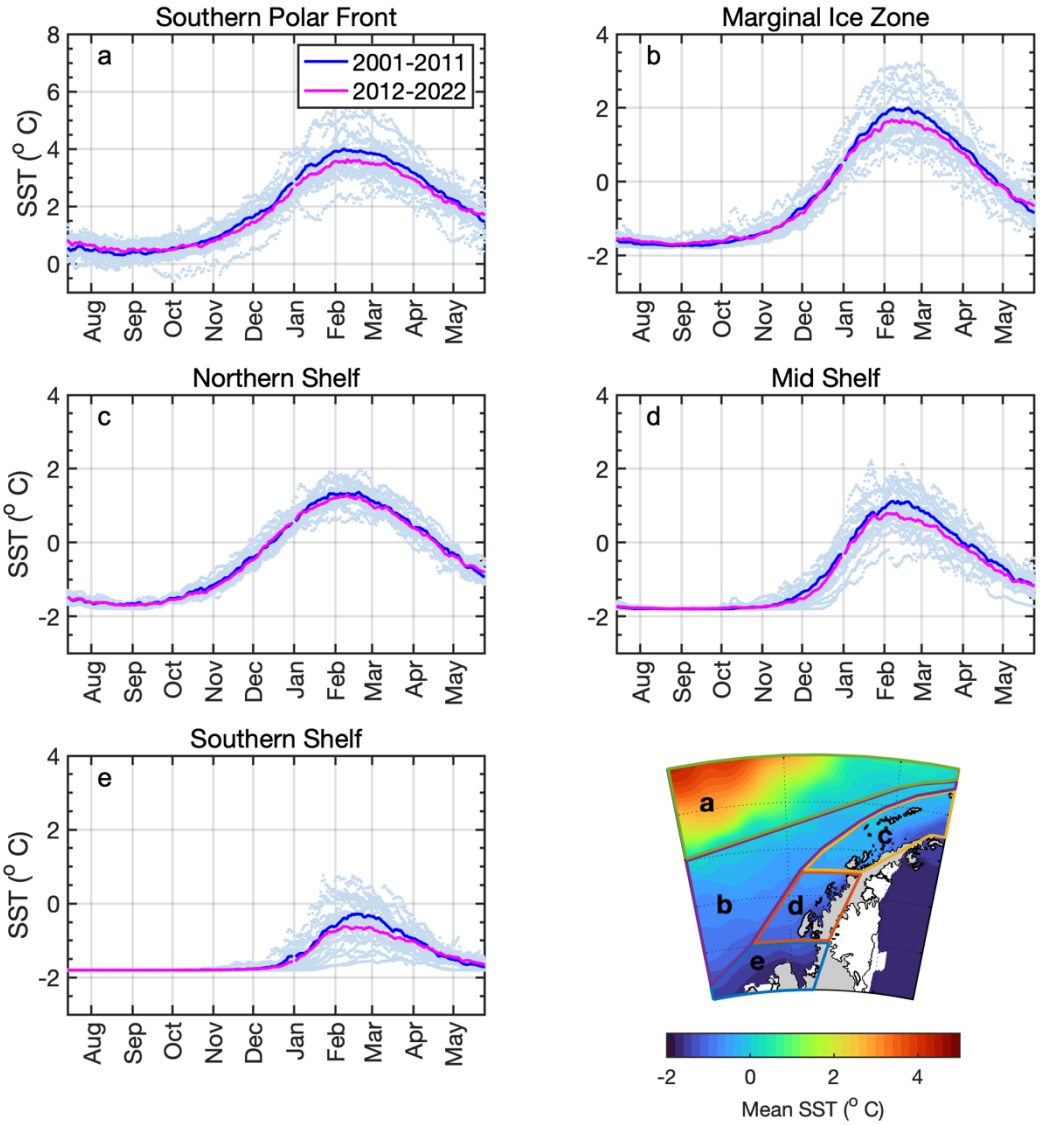

Fig. S16. Seasonal cycles of daily SST for two decades 2000-2010 (pink) vs. 2010-2020 (blue). Regions shown in map inset overlay long-term mean SST. Decades were not significantly different for any of the seasonal cycle ($p > 0.059$; Kruskal-wallis).

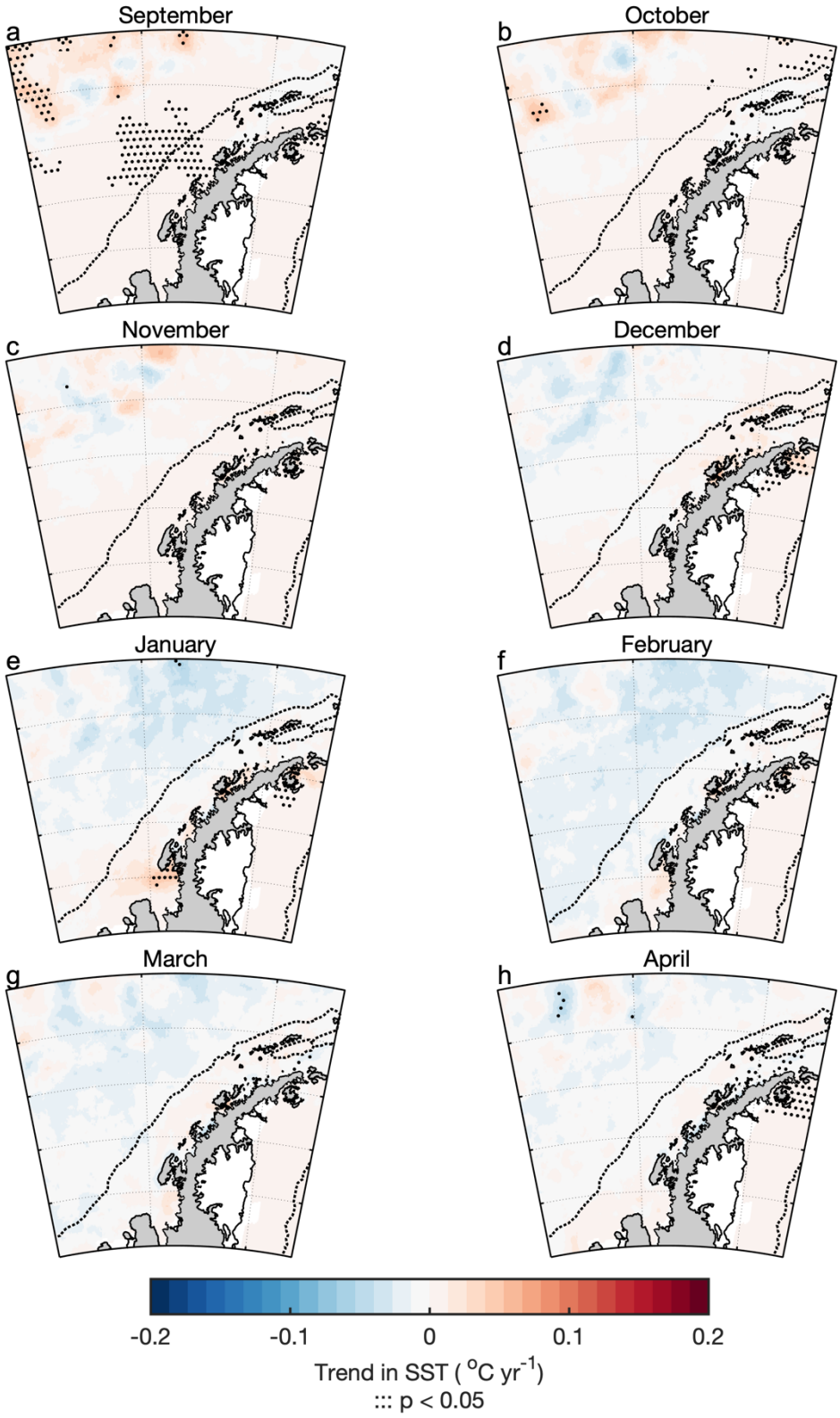

Fig. S17. Trends in SST for each month over the 24-year time series. Black dots indicate areas where trends are statistically significant ($p < 0.05$; Theil-Sen nonparametric estimator of slope). Black dotted line indicates the continental shelf break (1000 m isobath).

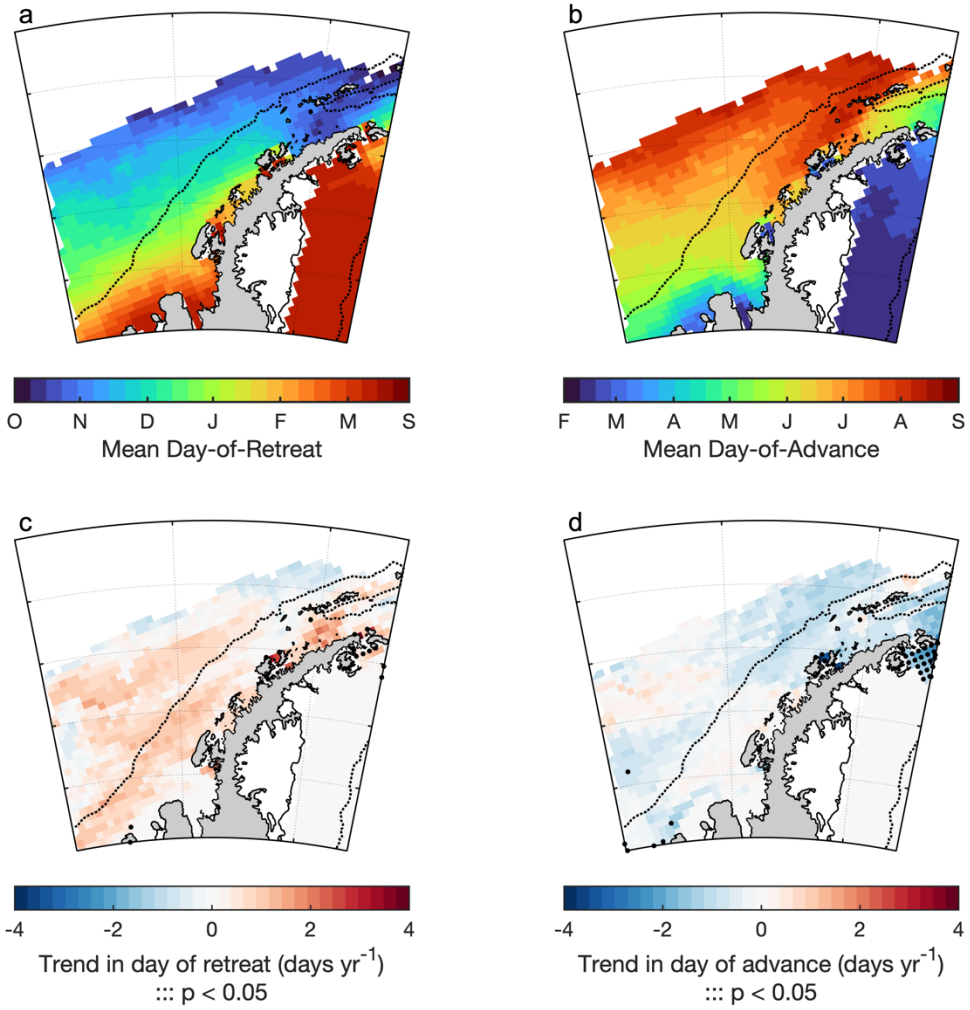

Fig. S18. Sea ice retreat date and advance date for 1997-2020, including a) mean day-of-retreat, b) mean day-of-advance, c) trend in day-of-retreat, and d) trend in day-of-advance. Day of retreat and advanced were calculated as in Stammerjohn et al. (2008) based on sea ice concentration derived from satellite imagery (Scanning Multichannel Microwave Radiometer and Special Sensor Microwave/Imager (SMMR-SSM/I)). Black dots in c) and d) indicate statistical significance. Trends in retreat date c) were statistically significant for only 0.5% of the x,y locations shown ($p < 0.045$; Theil-Sen nonparametric estimator of slope) and were not statistically significant for 99.5% of the locations shown ($p > 0.054$). Trends in advance date d) were statistically significant for only 1.2% of the x,y locations shown ($p < 0.049$; Theil-Sen nonparametric estimator of slope) and were not statistically significant for 98.8% of the locations shown ($p > 0.055$).

LITERATURE CITED

Dierssen, HM (2000) Ocean color remote sensing of chlorophyll and primary production west of the Antarctic Peninsula. PhD Dissertation. University of California Santa Barbara.

Dierssen, HM, Smith RC (2000) Bio-optical properties and remote sensing ocean color algorithms for Antarctic Peninsula waters. Journal of Geophysical Research **105**:26301–26312. doi:10.1029/1999JC000296

Greene CA, Thirumalai K, Kearney KA, and others (2019) The Climate Data Toolbox for MATLAB. Geochemistry, Geophysics, Geosystems **20**:3774–3781. doi:10.1029/2019GC008392

Montes-Hugo M, Doney SC, Ducklow HW, Fraser W, Martinson D, Stammerjohn SE, O Schofield (2009) Recent changes in phytoplankton communities associated with rapid regional climate change along the Western Antarctic Peninsula. Science **323**:1470–1473. doi:10.1126/science.1164533

Smith RC, Baker KS, Dustan P (1981) Fluorometer techniques for measurement of oceanic chlorophyll in the support of remote sensing. Visibility Laboratory, Scripps Institution of Oceanography, San Diego, CA. SIO Ref. 81-17.

Stammerjohn SE, Martinson DG, Smith RC, Yuan X, Rind D (2008) Trends in Antarctic annual sea ice retreat and advance and their relation to El Niño-Southern Oscillation and Southern Annular Mode variability. Journal of Geophysical Research: Oceans **113**. doi:10.1029/2007jc004269